

Probing criticality with deep learning in relativistic heavy-ion collisions

Yige Huang,¹ Long-Gang Pang,^{1,*} Xiaofeng Luo,^{1,†} and Xin-Nian Wang^{1,2,‡}

¹*Key Laboratory of Quark and Lepton Physics (MOE) & Institute of Particle Physics,
Central China Normal University, Wuhan 430079, China*

²*Nuclear Science Division, Lawrence Berkeley National Laboratory, Berkeley, CA 94720, USA*

Systems with different interactions could develop the same critical behaviour due to the underlying symmetry and universality. Using this principle of universality, we can embed critical correlations modeled on the 3D Ising model into the simulated data of heavy-ion collisions, hiding weak signals of a few inter-particle correlations within a large particle cloud. Employing a point cloud network with dynamical edge convolution, we are able to identify events with critical fluctuations through supervised learning, and pick out a large fraction of signal particles used for decision-making in each single event.

I. INTRODUCTION

Quantum Chromodynamics (QCD) is the fundamental theory of the strong interaction. Exploring the phase structure of strongly interacting QCD matter is one of the main goals of heavy-ion collision experiment [1–3]. Lattice QCD [4–6] predicts a smooth crossover transition from normal hadronic phase to Quark-Gluon Plasma (QGP) around temperature $T_c=156$ MeV at vanishing baryon chemical potential ($\mu_B = 0$ MeV). At finite baryon density region, QCD-based models calculations [7–10] indicate that there is a possible QCD critical point (CP), which is the end point of the first-order phase transition boundary between the hadronic matter and QGP.

Searching for the CP is one of the most important goals in beam energy scan (BES) program at the Relativistic Heavy-ion Collider (RHIC) [1–3]. Many theoretical and experimental efforts have been made to locate the CP [3, 11, 12]. One avenue is to classify the smooth crossover and first order phase transition using the information from the final state particle spectra and collective flow [13–25]. This method looks for the consequences of the softening of the equation of state since the pressure gradients are much smaller in a medium with a first order phase transition than a smooth crossover transition, which leads to slower fluid acceleration and smaller transverse momenta of final state particles. Another avenue is to search for the enhanced fluctuations when the system goes through the critical point. These includes, for example, fluctuations of conserved charges [26–33], hydrodynamic fluctuations [34–36], fluctuations caused by spinodal instabilities [37–47] and enhanced light nuclei yield ratio due to baryon density fluctuations [48–51].

Many critical phenomena in systems with different interactions can develop the same critical behaviour with a universality that is dictated by the symmetry of the systems and can be described by same critical exponents

[52]. Lee and Yang proved that the Ising model in a magnetic field and a lattice gas are mathematically equivalent [53]. Employing this universality, one can therefore map the QCD equation of state to that given by a 3-dimensional Ising model with the same universality class [11, 53–57] to study the QCD phase diagram. The divergence of the correlation length near the critical point will lead to the critical opalescence and scaling invariant, which means that the systems are self-similar when the resolution changes. One thus expects that particles from the freeze-out hyper-surface close to the critical point have multi-particle fractal structure in the momentum space [58–62]. Experimentally, intermittency analysis has been proposed to probe the self-similarity and density fluctuations in heavy-ion collisions. Though a non-trivial intermittency phenomenon is observed recently by the NA61/SHINE experiment at CERN SPS [63–65] in Ar+Sc collisions at 150 AGeV, the magnitude of background fluctuations is big and the power law scaling is not fully established. No intermittency signal is observed in C+C, Pb+Pb and Be+Be collisions with similar collision energies. Critical Monte Carlo simulations suggest a maximum critical proton fraction smaller than 0.3% in Be+Be collision, indicating that traditional intermittency analysis may fail in looking for the weak signal of self-similarity, if the fraction of CMC particles is small compared with uncorrelated background. It is interesting to explore whether the state-of-the-art deep learning can help to identify the weak intermittency signal from each event of heavy ion collisions.

Recently deep learning has been used to study the QCD equation of states by classifying phase transition types, using convolution neural network [66–69] and point cloud network [70, 71]. In heavy ion collisions at low energies, auto-encoder with a single latent variable is also used to study the order parameter of the nuclear liquid-gas phase transition [72]. In these studies, deep learning is powerful in mapping momentum or charge distributions of particles to the type of QCD phase transitions. In this study, we will train a dynamical edge convolution network plus a point cloud network to identify weak intermittency signals of critical fluctuations, from exotic uncorrelated background particles. Employ-

* lgpang@ccnu.edu.cn

† xfluo@ccnu.edu.cn

‡ xnwang@lbl.gov

ing Critical Monte Carlo (CMC) [61, 62], we encode the self-similarity in the inter-particle distances in momentum space. Further, we assume that only a small fraction of particles have intermittency which does not change the single particle distribution.

This paper is organized as follows. In Sec.II, we present the JAM transport model which is used to generate data on multiple particle production in heavy ion collisions. The CMC is used to generate intermittency signals of critical fluctuations and the deep neural network is used for both classification and tagging. In Sec. III, the prediction accuracy is compared for point cloud network and dynamical edge convolution neural network. We also show the performance of signal-particle tagging. In Sec. IV, we discuss and summarize the findings and the implications of the present work.

II. METHOD

Probing critical fluctuations in heavy-ion collisions is a typical inverse problem. The information of criticality should be transmitted through the dynamical evolution of the dense medium in heavy-ion collisions and get encoded in the final state hadrons that are recorded by detectors. In the forward process, relativistic hydrodynamics as well as hadronic transport model are widely used to generate single particle distribution and multi-hadron correlations. In the present study, we use a hadronic transport model JAM [73, 74] to generate background events without critical fluctuations. On the other hand, to introduce critical fluctuations, the so called Critical Monte-Carlo (CMC) model [61, 62] is applied to generate a series of correlated particle momentum, which will be used to replace the momentum of particles in JAM events.

In the inverse process, a point cloud network and a dynamical edge convolution network are trained to identify critical fluctuations from large amount of uncorrelated background particles. The traditional intermittency analysis is also carried out to probe the encoded critical signals in the JAM events and validate the effectiveness of the deep learning method.

A. The JAM and Critical Monte-Carlo model

JAM model is a hadronic transport model to simulate heavy-ion collisions [73–82]. It simulates the complicated process from initial stage nuclear collisions to multiple particle production and final state hadronic interactions. Independent binary collisions among hadrons including produced ones are modeled using the vacuum hadron-hadron scattering cross section. In the present study, the mean field mode of JAM model is used to generate background events without including the critical fluctuations.

To simulate events involving critical fluctuations, Critical Monte-Carlo (CMC) model [61, 62, 83] is used to generate

a series of correlated particle momentum according to a power law function:

$$f(\Delta p) = A\Delta p^{-\alpha} \quad (1)$$

where Δp is the distance of two CMC particles along an axis in momentum space. $\nu = 1/6$ is an index related to the universality class of Ising model, and we let $\alpha = 1 + \nu$. a and b are the minimum and maximum of Δp , and in our study, we set $a = 2 \times 10^{-7} \text{GeV}/c$ and $b = 2 \text{GeV}/c$. $A = (\nu a^\nu b^\nu)/(b^\nu - a^\nu)$, is the normalization coefficient which is independent of Δp . In this study, we only consider 2D momentum space (p_x, p_y) . The Levy flight random walk algorithm proposes the next step with strides respecting the distribution $f(\Delta p) = A\Delta p^{-\alpha}$ for Δp_x and Δp_y independently, and in this way, two sequence of p_x and p_y of CMC particles are generated whose adjacent differences Δp obey the power law distribution. The self-similarity or intermittency is thus encoded in these CMC particles, which is related to the observed large local density fluctuations associated with the critical point.

For such a probability density function $f(\Delta p) = A\Delta p^{-1-\nu}$ within a range of (a, b), it is possible to derive its cumulative distribution function:

$$F(\Delta p) = \frac{b^\nu(\Delta p^\nu - a^\nu)}{\Delta p^\nu(b^\nu - a^\nu)} \quad (2)$$

where $F(\Delta p)$ is the cumulative distribution function of random variable Δp , $F(\Delta p) = \int_a^b f(\Delta p)d\Delta p$. And one can then calculate the inverse function of $F(\Delta p)$:

$$\Delta p(F) = \left(\frac{a^\nu b^\nu}{b^\nu - b^\nu F + a^\nu F}\right)^{1/\nu} \quad (3)$$

By randomly picking up a F respecting to uniform distribution between 0 and 1, and using Eq. 3, one can obtain a Δp .

B. Data set preparation

We generate about 2.2×10^5 events of Au+Au central collisions at $\sqrt{s_{\text{NN}}} = 27 \text{ GeV}$ with impact parameters $b < 3 \text{ fm}$. Each event consists of hundreds of charged particles including pion, kaon and proton. The transverse momentum p_x and p_y are considered as two features of each particle. Therefore, each event stores one particle cloud in 2-dimensional momentum space. 2×10^5 events are used to form the training set, while the number of events for validation and test are 1×10^3 and 2×10^4 , respectively. For each JAM event, a corresponding CP event is created that encodes the critical fluctuation signals from CMC model. As a result, 4.4×10^5 events in total are used in our study. To avoid data pollution, event with critical fluctuations and its corresponding JAM event are always put in the same data category. In this case, if one JAM event is in the training data, the

event with critical fluctuations associated with that JAM event is also put in the training data. We will refer to these events with critical fluctuations as CP events and these particles encoded with the critical fluctuations as CMC particles. Since the CMC model only generates the momentum correlation pattern and does not include the information of specific particle species, we don't distinguish between the types of particles when performing the replacement of particle in a JAM event.

For a given JAM event, we use replacing rate $\eta = N_{CMC}/N_{JAM}$ to describe the multiplicity ratio of CMC events to JAM events, the number of CMC particles introduced into its corresponding CP event can reflect how strongly the critical signal is encoded. In our study, two kinds of CP events with $\eta = 5\%$ and $\eta = 10\%$, respectively, are prepared. The detailed replacing procedures are listed below:

1. Randomly select a particle in the chosen JAM event, use its (p_x, p_y) as the starting momentum for generating the CMC event.
2. Fill a histogram H of the transverse momentum distribution from the generated CMC event. Remark the maximum magnitude of this histogram as M .
3. Loop over the particles in the JAM events. For each particle, find its corresponding p_T bin in H , record the content of H in the p_T bin as f .
4. Get a random number y in range from 0 to M respecting to uniform distribution. If $y \leq f$, randomly select a CMC particle in the p_T bin and replace this JAM particle with it; and if $y > f$, give up this JAM particle and go back to step 3 to find next JAM particle.
5. Repeat step 3 to 4 until all the CMC particles are used or all the JAM particles are looped.

By applying such algorithm, it is possible to keep the p_T spectra of the substituted JAM particles close to that of the introduced CMC particles, hence the p_T spectra of the JAM event and the corresponding CP event are quit similar. Even if there has a fluctuation of p_T distribution, the overall p_T spectrum will not be greatly affected due to the small fraction of CMC particles (5% or 10%) in the CP event. Considering the momentum resolution of experimental detector, we introduced a uncertainty for momentum of each particle in JAM event with a smearing as $\delta p_i \approx \pm 0.05 p_i$, where $i = x, y$. The smearing operation will be done after the JAM and CP events are generated.

C. Intermittency analysis

Local density fluctuations near the QCD critical point can be probed by intermittency analysis of scaled factorial moments [62] in relativistic heavy-ion collisions. The

scaled factorial moments (SFM)[62] are defined as follows,

$$F_q(M) = \frac{\langle \frac{1}{M^D} \sum_{i=1}^{M^D} n_i(n_i-1) \cdots (n_i-q+1) \rangle}{\langle \frac{1}{M^D} \sum_{i=1}^{M^D} n_i \rangle^q} \quad (4)$$

where M is the number of grids in momentum space with equal size, D is the dimension, i is the number of particles in the i th momentum-grid, and q is the order of the SFM method.

When M is large, the power law dependence of SFM on the number of partitioned bins implies a self-similar correlations in the studied system[58, 84].

$$F_q(M) \approx (M^D)^{\phi_q} \quad (5)$$

The intermittency index ϕ_q can characterize the strength of intermittency behavior and is related to the anomalous fractal dimension of the system[85]. And there are studies show that using intermittency measurement together with the estimated freeze-out parameters can estimate the possible critical region of the QCD CEP[86].

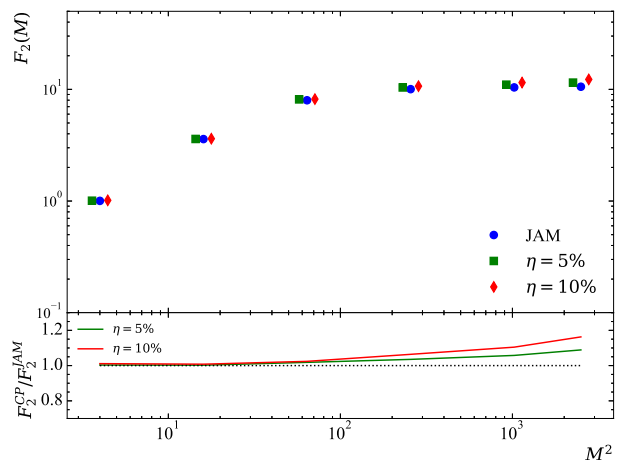


FIG. 1. The second order scaled factorial moments analysis for uncorrelated JAM events and events with critical fluctuations. The upper-panel shows the absolute values of SFM for JAM events and events with 5% and 10% CMC particles. To avoid the overlap of markers, results of critical events are slightly shifted horizontally for a clearer visualization. The lower-panel shows the ratios between critical and normal JAM events. No significant differences are observed for the absolute SFM values and their ratios.

In the present study, the second order SFM ($q = 2$) in two dimensional space ($D = 2$) are studied for $M = 2, 4, 8, 16, 32, 50$. As we take the experimental detectors into consideration, in SFM calculation, we only take no more than 50 grids for each dimension in a range of plus-minus 2.5 GeV/c to keep p_T resolution to be like experimental options and at about 0.1 GeV/c.

As shown in Figure. 1, the intermittency analysis using the SFM method [62–65] can not differentiate CP events

with 5% and 10% CMC particles that carry critical fluctuations from uncorrelated JAM events.

D. Dynamical edge convolution neural network

A graph-based dynamical edge convolution neural network is trained for our multi-task learning. The input to the neural network are the particle cloud of each event, which consists of a list of particles with their information on (p_x, p_y) . The output of the neural network corresponds to two tasks. The first task is the binary classification which requires true labels of each single event for supervised learning, with CP indicating events with critical fluctuations and JAM indicating events without. The second task is the particle tagging which requires true labels of each single particle, with 0 or 1 to indicate whether the particle is generated using Critical Monte Carlo model.

Shown in Figure. 2 is the architecture of our neural network. There are two kNN plus dynamical edge convolution blocks connecting to the input layer. In the first block, kNN is used to find the k-nearest neighbors of each particle in (p_x, p_y) space. A fully connected network is used to learn edge features $\phi(\vec{p}_i, \vec{p}_j)$ between the i 'th particle and its j 'th neighbor. This module is shared by all its neighbors of particle i to produced edge features and that explains the name "edge convolution". The information of particle i together with its edge features are feed to the second block. Edge convolution layer would not only make use of the features of input neuron itself, but also take the relevance between the clustered units near that neuron into consideration, thus it can effectively capture the correlation information between particles.

The second kNN find the k-nearest neighbors of each particle in feature space. It is thus possible to correlate particles that are far away in momentum space. The neighbors of each particle change dynamically when the distances are computed in feature space, that is why the method is called "dynamical edge convolution".

The features of each particle together with its "local" information are flattened and feed to a fully connected neural network to get a high dimensional latent variable for each particle. The latent variable provides a high dimensional representation of each particle. The above neural network is also shared by all particles and is called 1D convolution neural network (CNN). Finally, the latent variables of each particle are used for two different tasks. The module of "Classification" task is shown in the lower right corner. A global max pooling gets the maximum values of each feature among all particles. This symmetric permutation operation learns the global feature of each particle cloud and is used to determine whether it is a CP or JAM event. The module of "Tagging" task is shown on the right of Figure. 2. A 1D CNN with one output neuron is used to tag each particle in the particle cloud. This module provides interpretation on whether the correlated particles are used to identify events with

critical fluctuations. We have labeled correlated CMC particles as "signal" and uncorrelated JAM particles as "noise". Binary cross entropy is used to compute the differences between the tagging output and the true labels of each particle. The loss values of tagging module is added to the total loss with a weighting factor 10^{-3} such that the network focus more on "classification" task.

For comparison, we also train a point-cloud network without the kNN and dynamical edge convolution blocks shown in Figure. 2. The (p_x, p_y) of each particle is directly feed to 1D CNN with 256, 128 and 64 channels respectively for classification. Global average pooling layer is used in this simple point-cloud network as it performs better here. Without kNN and dynamical edge convolution, the network can not capture much local information for intermittency identification.

III. RESULTS AND DISCUSSION

A. Classification accuracy

Shown in the Figure. 3 are the training (solid lines) and validation (dashed lines) accuracy as a function of training epochs. Both training and validation accuracy increase as the model is trained longer with more epochs. The validation accuracy reaches a maximum of 99.3%, which means that deep learning is able to classify each single event with high accuracy, for uncorrelated JAM events and events mixed with 90% uncorrelated JAM particles and 10% CMC particles ($\eta = 10\%$). For a smaller replacing rate ($\eta = 5\%$), both validation and training accuracy decrease as compared with ($\eta = 10\%$), whose maximum value is about 93.3%. Note: the smeared 5% and 10% both got 93.3% acc. for validation set, while the 10% one got higher score for test set. The validation accuracy is slightly higher than training accuracy caused by the dropout and batch normalization layers used in the network. These two kinds of layers are known to be able to increase the generalization of the network by introducing noise during training.

Shown in Table. I are the testing accuracy of four different configurations. Using the dynamical edge convolution plus point cloud network we constructed in this study, the testing accuracy are 97.7% for 10% replacing rate and 92.8% for 5% replacing rate, which are not quite far away from the validation accuracy. Removing the dynamical edge convolution block, we have tested the performance of the point cloud network with varying numbers of layers and neurons per layer to get the best testing accuracy. The testing accuracy decreases to 84.8% for 10% replacing rate and 83.4% for 5% replacing rate.

Another test set is prepared to make sure that the network make their decision based on multi-particle correlation in the CMC particles. In this test set, 5% or 10% particles of a JAM event are replaced by same amount of particles sampled randomly from many other events,

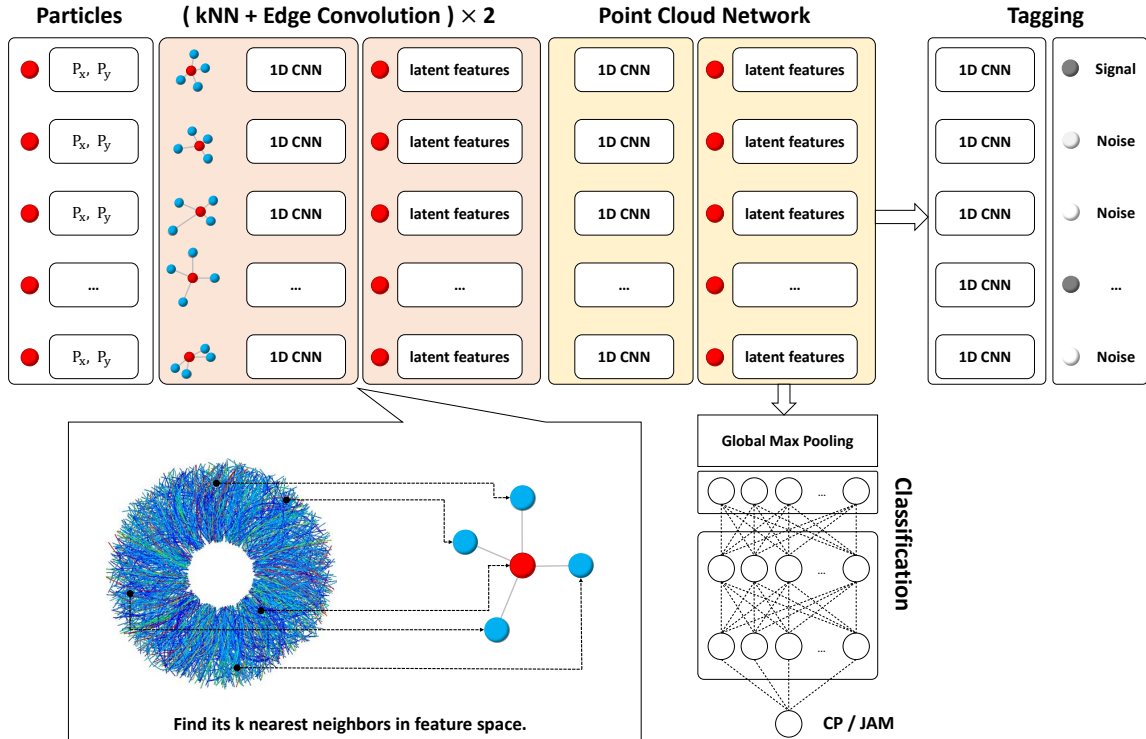


FIG. 2. Dynamical edge convolution neural network with point cloud module for both classification and tagging. The edge convolution block looks for k nearest neighbors of each particle to obtain a latent representation of that very particle, with short or long range correlations encoded deeply in. The representation of each particle are used in two tasks. One is the classification task to identify critical fluctuations from uncorrelated background events. The other is the tagging task to label correlated particles used for decision making.

Testing accuracy		
η	Edge-Conv	Point-Cloud Net
5%	92.8%	83.4%
10%	97.7%	84.8%

TABLE I. The testing accuracy for dynamical edge convolution network and a simple point cloud network.

one particle from each event to eliminate the two particle correlation in the replaced particles. If our network trained to identify CMC particles is fooled to classify these mixed events as CMC events, it means that the network learns the missing correlation in the replaced particles as compared with original JAM particles. In practice, our trained network treat these mixed events as JAM events, which is a proof that the network make their predictions using signals of CMC particles.

B. Interpretability: tagging

To figure out how does the network make its decision in identifying critical fluctuations from the background, we have added a tagging layer to the neural network. To quantify the tagging performance, we introduce two

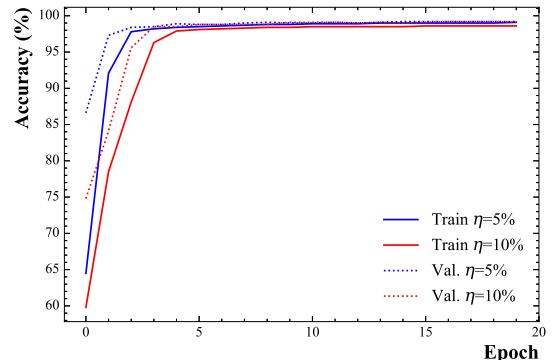


FIG. 3. The training and validation accuracy as a function of epochs. The training accuracy is in solid lines, for replacing rate 5% (blue) and 10%(red). The validation accuracy is in dashed lines for replacing rate 5% and 10%.

metrics as follows,

$$r_c = \frac{N_C}{N_C + N_M}, \quad r_t = \frac{N_C}{N_C + N_W} \quad (6)$$

where r_c is the catching rate defined as the ratio between the number of correctly tagged particles N_C and total

number of signal particles $N_C + N_M$, where N_M is the number of signal particles missed by the tagging module. r_t is the tagging rate defined as the ratio between the number of correctly tagged particles N_C and the total number of tagged particles $N_C + N_W$, where N_W is the number of wrongly tagged uncorrelated particles.

The average catching rates $r_c = 73.6\%$ for $\eta = 5\%$ and $r_c = 75.9\%$ for $\eta = 10\%$ indicate that the network may use about 3/4 of the correlated particles to make its decision. On the other hand, the tagging rate $r_t = 94.5\%$ for $\eta = 5\%$ and $r_t = 95.4\%$ for $\eta = 10\%$ are much higher than catching rate r_c . This result tells us that the tagging module can label CMC particles quite precisely.

Since both edge convolution and the following 1D convolution layers of tagging module perform the same transformation for each particle, we can reversely track the tensor of labeled particles in the hidden feature space in the forward propagation process of neural network. For each input CP event, by checking the feature space after passing edge convolution layer, for a total of N CMC particles well tagged, we find the k nearest particles in the feature space corresponding to the feature vector of each particle, and count the number M of CMC particles that were also well tagged. The proportion of those well tagged CMC particles from kNN to the total number of these kNN particles can then be calculated as $\frac{M}{k \times N} = 94\%$. This result indicates that, the feature space transformation guided by edge convolution can aggregate CMC particles into a cluster in the new feature space, and then the tagging module can label them through the subsequent 1D convolution layers.

Figure 4 demonstrates the output of the tagging module. In the upper subplots, grey dots represent unchanged JAM particles and red dots represent all the CMC particles in two testing events. The corresponding tagging output for these two events are shown in the two lower subplots, where the red dots represent CMC particles correctly tagged by the network while the blue ones are JAM particles but incorrectly tagged as CMC particles. In average, 3/4 of CMC particles are recognized by the tagging module. And as discussed before, the incorrectly tagged particles are much fewer than correctly tagged CMC particles. The two figures in the left are for 5% replacing rate while the ones on the right are for 10% replacing rate.

Figure 5 shows the SFM calculation of $\eta = 5\%$ CP events and the SFM of tagged particles of them, the former ones event have no increment with the increase of M^2 while the tagged ones present slight power law. This result reflects that the tagging module can somehow extract the encoded intermittency information.

IV. SUMMARY AND OUTLOOK

In summary, we have constructed a dynamical edge convolution plus point cloud network to identify the weak intermittency signal from the experimental data of

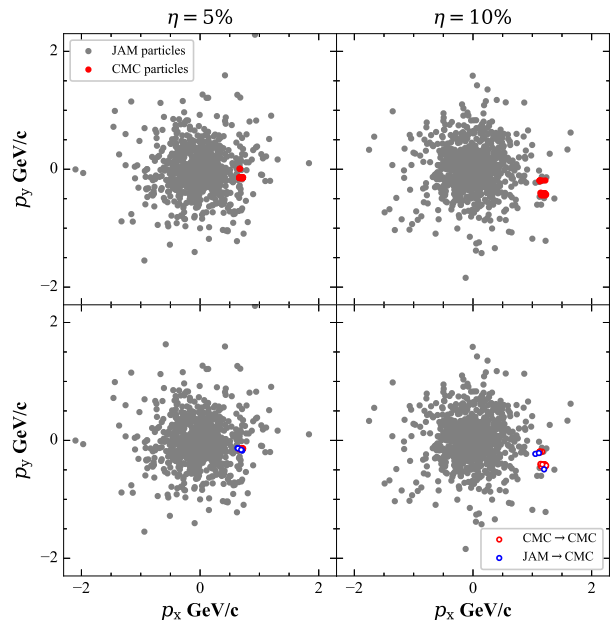


FIG. 4. The upper subplots show the comparison of JAM event and its corresponding CP event, in which the grey dots are the unchanged JAM particles, and the red ones are the critical particles introduced by CMC events. The lower subplots are labeled results of tagging network, and the red dots refer to particles which were tagged correctly, while the blue ones are JAM particles labeled as CMC ones, while the grey dots are unlabeled particles. The graphs on the left show an example of $\eta = 5\%$, while the ones on the right show an example of $\eta = 10\%$. Although the CMC clusters in the two examples shown are all distributed on the right side of phase space, the location of CMC particles are not restricted indeed and they can be on any corner of the plot.

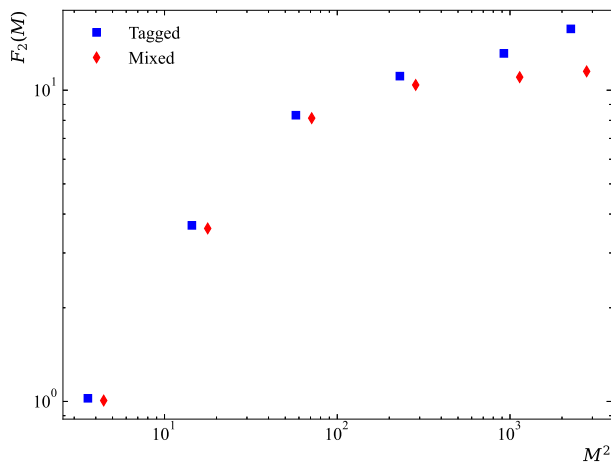


FIG. 5. The 'Mixed' labeled red diamond markers represent the SFM results of all particles from $\eta=5\%$ CP events, while the 'Tagged' labeled blue square markers stand for the SFM of tagged part of those events. As M^2 increase, the red diamonds have a flat performance, and the blue squares show a increment.

heavy-ion collisions. We have demonstrated that such a state-of-the-art deep learning network enables us to achieve a testing accuracy 92.8% if only 5% of JAM particles in each event are replaced by correlated CMC particles. The performance increases to 97.7% if the replacing rate of correlated particles increases to 10%. Removing the dynamical edge convolution block will decrease the performance by a large margin. Using tagging module, we further demonstrate that the network can use around 3/4 of correlated particles to make their decision. At the same time, only about 5% of uncorrelated background particles are incorrectly tagged as CMC particles.

We observe that the network can identify self-similarity or scaling invariant from uncorrelated background. This is important for experimental data analysis since only one indication of intermittency is observed in Ar + Sc collisions whereas several other systems with similar collision energies fail. Different from previous theoretical studies, we preserve the single particle distribution while introducing a small fraction of particles with multi particle fractal structure. This is more realistic but also difficult for the traditional intermittency analysis. Based on our study, deep learning shows strong pattern recognition ability in identifying weak intermittency signals associated with critical phenomena. The method devel-

oped in this study can be applied to probe the critical fluctuations in heavy-ion collisions and can also be used to explore the criticality of other systems.

ACKNOWLEDGEMENT

We thank Jin Wu for helpful discussions on the critical monte carlo model. This work is supported by the National Key Research and Development Program of China (Grant No. 2020YFE0202002 and 2018YFE0205201), the National Natural Science Foundation of China under Grant Nos. 12122505, 11935007, 11221504, 11890711, 11861131009 and 12075098, and by the Director, Office of Energy Research, Office of High Energy and Nuclear Physics, Division of Nuclear Physics, of the U.S. Department of Energy (DOE) under grant No. DE-AC02-05CH11231, by the U.S. National Science Foundation under No. OAC-2004571 within the X-SCAPE Collaboration. Computations are performed at Nuclear Science Computer Center at CCNU (NSC3). LG Pang and YG Huang also acknowledge the support provided by Huawei Technologies Co., Ltd.

-
- [1] Kenji Fukushima and Tetsuo Hatsuda, “The phase diagram of dense QCD,” *Rept. Prog. Phys.* **74**, 014001 (2011), arXiv:1005.4814 [hep-ph].
- [2] Adam Bzdak, Shinichi Esumi, Volker Koch, Jinfeng Liao, Mikhail Stephanov, and Nu Xu, “Mapping the Phases of Quantum Chromodynamics with Beam Energy Scan,” *Phys. Rept.* **853**, 1–87 (2020), arXiv:1906.00936 [nucl-th].
- [3] Xiaofeng Luo and Nu Xu, “Search for the QCD Critical Point with Fluctuations of Conserved Quantities in Relativistic Heavy-Ion Collisions at RHIC : An Overview,” *Nucl. Sci. Tech.* **28**, 112 (2017), arXiv:1701.02105 [nucl-ex].
- [4] Y. Aoki, Szabolcs Borsanyi, Stephan Durr, Zoltan Fodor, Sandor D. Katz, Stefan Krieg, and Kalman K. Szabo, “The QCD transition temperature: results with physical masses in the continuum limit II,” *JHEP* **06**, 088 (2009), arXiv:0903.4155 [hep-lat].
- [5] H. T. Ding et al. (HotQCD), “Chiral Phase Transition Temperature in (2+1)-Flavor QCD,” *Phys. Rev. Lett.* **123**, 062002 (2019), arXiv:1903.04801 [hep-lat].
- [6] Heng-Tong Ding, Frithjof Karsch, and Swagato Mukherjee, “Thermodynamics of strong-interaction matter from Lattice QCD,” *Int. J. Mod. Phys. E* **24**, 1530007 (2015), arXiv:1504.05274 [hep-lat].
- [7] Chao Shi, Yong-Long Wang, Yu Jiang, Zhu-Fang Cui, and Hong-Shi Zong, “Locate QCD Critical End Point in a Continuum Model Study,” *JHEP* **07**, 014 (2014), arXiv:1403.3797 [hep-ph].
- [8] Fei Gao and Yu-xin Liu, “QCD phase transitions via a refined truncation of Dyson-Schwinger equations,” *Phys. Rev. D* **94**, 076009 (2016), arXiv:1607.01675 [hep-ph].
- [9] Christian S. Fischer, “QCD at finite temperature and chemical potential from Dyson-Schwinger equations,” *Prog. Part. Nucl. Phys.* **105**, 1–60 (2019), arXiv:1810.12938 [hep-ph].
- [10] Wei-jie Fu, Jan M. Pawłowski, and Fabian Rennecke, “QCD phase structure at finite temperature and density,” *Phys. Rev. D* **101**, 054032 (2020), arXiv:1909.02991 [hep-ph].
- [11] Mikhail A. Stephanov, “QCD phase diagram and the critical point,” *Prog. Theor. Phys. Suppl.* **153**, 139–156 (2004), arXiv:hep-ph/0402115.
- [12] M. A. Stephanov, “QCD phase diagram: An Overview,” *PoS LAT2006*, 024 (2006), arXiv:hep-lat/0701002.
- [13] J. Hofmann, Horst Stoecker, Ulrich W. Heinz, W. Scheid, and W. Greiner, “Possibility of Detecting Density Isomers in High Density Nuclear MACH Shock Waves,” *Phys. Rev. Lett.* **36**, 88–91 (1976).
- [14] Horst Stoecker and W. Greiner, “High-Energy Heavy Ion Collisions: Probing the Equation of State of Highly Excited Hadronic Matter,” *Phys. Rept.* **137**, 277–392 (1986).
- [15] J. Brachmann, S. Soff, A. Dumitru, Horst Stoecker, J. A. Maruhn, W. Greiner, L. V. Bravina, and D. H. Rischke, “Antiflow of nucleons at the softest point of the EoS,” *Phys. Rev. C* **61**, 024909 (2000), arXiv:nucl-th/9908010.
- [16] J. Brachmann, A. Dumitru, Horst Stoecker, and W. Greiner, “The Directed flow maximum near $c(s) = 0$,” *Eur. Phys. J. A* **8**, 549–552 (2000), arXiv:nucl-th/9912014.
- [17] L. P. Csernai and D. Rohrlich, “Third flow component as QGP signal,” *Phys. Lett. B* **458**, 454 (1999), arXiv:nucl-th/9908034.

- [18] Yu. B. Ivanov, E. G. Nikonov, W. Noerenberg, A. A. Shanenko, and V. D. Toneev, “Directed flow of baryons in heavy ion collisions,” *Acta Phys. Hung. A* **15**, 117–130 (2002), [arXiv:nucl-th/0011004](#).
- [19] Dirk H. Rischke, Yaris Pursun, Joachim A. Maruhn, Horst Stoecker, and Walter Greiner, “The Phase transition to the quark - gluon plasma and its effects on hydrodynamic flow,” *Acta Phys. Hung. A* **1**, 309–322 (1995), [arXiv:nucl-th/9505014](#).
- [20] Horst Stoecker, “Collective flow signals the quark gluon plasma,” *Nucl. Phys. A* **750**, 121–147 (2005), [arXiv:nucl-th/0406018](#).
- [21] L. P. Csernai, A. Anderlik, Cs. Anderlik, V. K. Magas, E. Molnar, A. Nyiri, D. Rohrich, and K. Tamosiunas, “The 3rd flow component as a QGP signal,” *Acta Phys. Hung. A* **22**, 181–186 (2005), [arXiv:hep-ph/0405277](#).
- [22] Yasushi Nara, Harri Niemi, Jan Steinheimer, and Horst Stöcker, “Equation of state dependence of directed flow in a microscopic transport model,” *Phys. Lett. B* **769**, 543–548 (2017), [arXiv:1611.08023 \[nucl-th\]](#).
- [23] Yasushi Nara, Harri Niemi, Akira Ohnishi, Jan Steinheimer, Xiaofeng Luo, and Horst Stöcker, “Enhancement of elliptic flow can signal a first order phase transition in high energy heavy ion collisions,” *Eur. Phys. J. A* **54**, 18 (2018), [arXiv:1708.05617 \[nucl-th\]](#).
- [24] Yasushi Nara, Jan Steinheimer, and Horst Stoecker, “The enhancement of v_4 in nuclear collisions at the highest densities signals a first-order phase transition,” *Eur. Phys. J. A* **54**, 188 (2018), [arXiv:1809.04237 \[nucl-th\]](#).
- [25] K. Paech, Horst Stoecker, and A. Dumitru, “Hydrodynamics near a chiral critical point,” *Phys. Rev. C* **68**, 044907 (2003), [arXiv:nucl-th/0302013](#).
- [26] M. A. Stephanov, “Non-Gaussian fluctuations near the QCD critical point,” *Phys. Rev. Lett.* **102**, 032301 (2009), [arXiv:0809.3450 \[hep-ph\]](#).
- [27] M. A. Stephanov, “On the sign of kurtosis near the QCD critical point,” *Phys. Rev. Lett.* **107**, 052301 (2011), [arXiv:1104.1627 \[hep-ph\]](#).
- [28] M. M. Aggarwal et al. (STAR), “Higher Moments of Net-proton Multiplicity Distributions at RHIC,” *Phys. Rev. Lett.* **105**, 022302 (2010), [arXiv:1004.4959 \[nucl-ex\]](#).
- [29] L. Adamczyk et al. (STAR), “Energy Dependence of Moments of Net-proton Multiplicity Distributions at RHIC,” *Phys. Rev. Lett.* **112**, 032302 (2014), [arXiv:1309.5681 \[nucl-ex\]](#).
- [30] L. Adamczyk et al. (STAR), “Beam-energy dependence of charge separation along the magnetic field in Au+Au collisions at RHIC,” *Phys. Rev. Lett.* **113**, 052302 (2014), [arXiv:1404.1433 \[nucl-ex\]](#).
- [31] L. Adamczyk et al. (STAR), “Collision Energy Dependence of Moments of Net-Kaon Multiplicity Distributions at RHIC,” *Phys. Lett. B* **785**, 551–560 (2018), [arXiv:1709.00773 \[nucl-ex\]](#).
- [32] J. Adam et al. (STAR), “Nonmonotonic Energy Dependence of Net-Proton Number Fluctuations,” *Phys. Rev. Lett.* **126**, 092301 (2021), [arXiv:2001.02852 \[nucl-ex\]](#).
- [33] Mohamed Abdallah et al. (STAR), “Cumulants and correlation functions of net-proton, proton, and antiproton multiplicity distributions in Au+Au collisions at energies available at the BNL Relativistic Heavy Ion Collider,” *Phys. Rev. C* **104**, 024902 (2021), [arXiv:2101.12413 \[nucl-ex\]](#).
- [34] Marlene Nahrgang, Stefan Leupold, Christoph Herold, and Marcus Bleicher, “Nonequilibrium chiral fluid dynamics including dissipation and noise,” *Phys. Rev. C* **84**, 024912 (2011), [arXiv:1105.0622 \[nucl-th\]](#).
- [35] Christoph Herold, Marlene Nahrgang, Igor Mishustin, and Marcus Bleicher, “Chiral fluid dynamics with explicit propagation of the Polyakov loop,” *Phys. Rev. C* **87**, 014907 (2013), [arXiv:1301.1214 \[nucl-th\]](#).
- [36] Christopher Plumberg and Joseph I. Kapusta, “Hydrodynamic fluctuations near a critical endpoint and Hanbury-Brown–Twiss interferometry,” *Phys. Rev. C* **95**, 044910 (2017), [arXiv:1702.01368 \[nucl-th\]](#).
- [37] Feng Li and Che Ming Ko, “Spinodal instabilities of baryon-rich quark-gluon plasma in the Polyakov–Nambu–Jona-Lasinio model,” *Phys. Rev. C* **93**, 035205 (2016), [arXiv:1601.00026 \[nucl-th\]](#).
- [38] O. Scavenius, A. Dumitru, E. S. Fraga, J. T. Lenaghan, and A. D. Jackson, “First order chiral phase transition in high-energy collisions: Can nucleation prevent spinodal decomposition?” *Phys. Rev. D* **63**, 116003 (2001), [arXiv:hep-ph/0009171](#).
- [39] Leticia F. Palhares and Eduardo S. Fraga, “Droplets in the cold and dense linear sigma model with quarks,” *Phys. Rev. D* **82**, 125018 (2010), [arXiv:1006.2357 \[hep-ph\]](#).
- [40] Christoph Herold, Marlene Nahrgang, Igor Mishustin, and Marcus Bleicher, “Formation of droplets with high baryon density at the QCD phase transition in expanding matter,” *Nucl. Phys. A* **925**, 14–24 (2014), [arXiv:1304.5372 \[nucl-th\]](#).
- [41] Feng Li and Che Ming Ko, “Spinodal instabilities of baryon-rich quark matter in heavy ion collisions,” *Phys. Rev. C* **95**, 055203 (2017), [arXiv:1606.05012 \[nucl-th\]](#).
- [42] Philippe Chomaz, Maria Colonna, and Jorgen Randrup, “Nuclear spinodal fragmentation,” *Phys. Rept.* **389**, 263–440 (2004).
- [43] Jorgen Randrup, “Spinodal decomposition during the hadronization stage at RHIC?” *Phys. Rev. Lett.* **92**, 122301 (2004), [arXiv:hep-ph/0308271](#).
- [44] C. Sasaki, B. Friman, and K. Redlich, “Density fluctuations in the presence of spinodal instabilities,” *Phys. Rev. Lett.* **99**, 232301 (2007), [arXiv:hep-ph/0702254](#).
- [45] Jan Steinheimer and Jorgen Randrup, “Spinodal amplification of density fluctuations in fluid-dynamical simulations of relativistic nuclear collisions,” *Phys. Rev. Lett.* **109**, 212301 (2012), [arXiv:1209.2462 \[nucl-th\]](#).
- [46] Jan Steinheimer and Jorgen Randrup, “Spinodal density enhancements in simulations of relativistic nuclear collisions,” *Phys. Rev. C* **87**, 054903 (2013), [arXiv:1302.2956 \[nucl-th\]](#).
- [47] Jan Steinheimer, Jørgen Randrup, and Volker Koch, “Non-equilibrium phase transition in relativistic nuclear collisions: Importance of the equation of state,” *Phys. Rev. C* **89**, 034901 (2014), [arXiv:1311.0999 \[nucl-th\]](#).
- [48] Kai-Jia Sun, Lie-Wen Chen, Che Ming Ko, Jie Pu, and Zhangbu Xu, “Light nuclei production as a probe of the QCD phase diagram,” *Phys. Lett. B* **781**, 499–504 (2018), [arXiv:1801.09382 \[nucl-th\]](#).
- [49] Ning Yu, Dingwei Zhang, and Xiaofeng Luo, “Search for QCD critical point by transverse velocity dependence of anti-deuteron to deuteron ratio,” *Chin. Phys. C* **44**, 014002 (2020), [arXiv:1812.04291 \[nucl-th\]](#).
- [50] Kai-Jia Sun, Che Ming Ko, Feng Li, Jun Xu, and Lie-Wen Chen, “Enhanced yield ratio of light nuclei in heavy ion collisions with a first-order chiral phase transition,” *Eur. Phys. J. A* **57**, 313 (2021), [arXiv:2006.08929 \[nucl-th\]](#).

- th].
- [51] Wenbin Zhao, Kai-jia Sun, Che Ming Ko, and Xiaofeng Luo, “Multiplicity scaling of light nuclei production in relativistic heavy-ion collisions,” *Phys. Lett. B* **820**, 136571 (2021), [arXiv:2105.14204 \[nucl-th\]](#).
- [52] K. G. Wilson and John B. Kogut, “The Renormalization group and the epsilon expansion,” *Phys. Rept.* **12**, 75–199 (1974).
- [53] T. D. Lee and Chen-Ning Yang, “Statistical theory of equations of state and phase transitions. 2. Lattice gas and Ising model,” *Phys. Rev.* **87**, 410–419 (1952).
- [54] Maneesha Sushama Pradeep and Mikhail Stephanov, “Universality of the critical point mapping between Ising model and QCD at small quark mass,” *Phys. Rev. D* **100**, 056003 (2019), [arXiv:1905.13247 \[hep-ph\]](#).
- [55] J. M. Karthein, D. Mroczek, A. R. Nava Acuna, J. Noronha-Hostler, P. Parotto, D. R. P. Price, and C. Ratti, “Strangeness-neutral equation of state for QCD with a critical point,” *Eur. Phys. J. Plus* **136**, 621 (2021), [arXiv:2103.08146 \[hep-ph\]](#).
- [56] Derek Teaney, “Dynamics of Critical Fluctuations in Nucleus-Nucleus Collisions,” *Nucl. Phys. A* **1005**, 121750 (2021).
- [57] Marcus Bluhm et al., “Dynamics of critical fluctuations: Theory – phenomenology – heavy-ion collisions,” *Nucl. Phys. A* **1003**, 122016 (2020), [arXiv:2001.08831 \[nucl-th\]](#).
- [58] A. Bialas and Robert B. Peschanski, “Intermittency in Multiparticle Production at High-Energy,” *Nucl. Phys. B* **308**, 857–867 (1988).
- [59] Helmut Satz, “Intermittency and Critical Behavior,” *Nucl. Phys. B* **326**, 613–618 (1989).
- [60] Rudolph C. Hwa, “Fractal Measures in Multiparticle Production,” *Phys. Rev. D* **41**, 1456 (1990).
- [61] N. G. Antoniou, Y. F. Contoyiannis, F. K. Diakonos, A. I. Karanikas, and C. N. Ktorides, “Pion production from a critical QCD phase,” *Nucl. Phys. A* **693**, 799–824 (2001), [arXiv:hep-ph/0012164](#).
- [62] Jin Wu, Yufu Lin, Yuanfang Wu, and Zhiming Li, “Probing QCD critical fluctuations from intermittency analysis in relativistic heavy-ion collisions,” *Phys. Lett. B* **801**, 135186 (2020), [arXiv:1901.11193 \[nucl-th\]](#).
- [63] T. Anticic et al. (NA49), “Critical fluctuations of the proton density in A+A collisions at 158A GeV,” *Eur. Phys. J. C* **75**, 587 (2015), [arXiv:1208.5292 \[nucl-ex\]](#).
- [64] Nikolaos Davis (NA61/SHINE), “Searching for the critical point of strongly interacting matter in nucleus-nucleus collisions at CERN SPS,” *PoS EPS-HEP2019*, 305 (2020).
- [65] Nikolaos Davis, Nikolaos Antoniou, and Fotios K. Diakonos (NA61/Shine), “Recent results from proton intermittency analysis in nucleus-nucleus collisions from NA61/SHINE at CERN SPS,” *PoS CORFU2018*, 154 (2019).
- [66] Long-Gang Pang, Kai Zhou, Nan Su, Hannah Petersen, Horst Stöcker, and Xin-Nian Wang, “An equation-of-state-meter of quantum chromodynamics transition from deep learning,” *Nature Commun.* **9**, 210 (2018), [arXiv:1612.04262 \[hep-ph\]](#).
- [67] Long-Gang Pang, “Machine learning for high energy heavy ion collisions,” *Nucl. Phys. A* **1005**, 121972 (2021).
- [68] Yi-Lun Du, Kai Zhou, Jan Steinheimer, Long-Gang Pang, Anton Motornenko, Hong-Shi Zong, Xin-Nian Wang, and Horst Stöcker, “Identifying the nature of the QCD transition in relativistic collision of heavy nuclei with deep learning,” *Eur. Phys. J. C* **80**, 516 (2020), [arXiv:1910.11530 \[hep-ph\]](#).
- [69] Yu. Kvasiuk, E. Zabrodin, L. Bravina, I. Didur, and M. Frolov, “Classification of Equation of State in Relativistic Heavy-Ion Collisions Using Deep Learning,” *JHEP* **07**, 133 (2020), [arXiv:2004.14409 \[nucl-th\]](#).
- [70] Jan Steinheimer, Longgang Pang, Kai Zhou, Volker Koch, Jørgen Randrup, and Horst Stoecker, “A machine learning study to identify spinodal clumping in high energy nuclear collisions,” *JHEP* **12**, 122 (2019), [arXiv:1906.06562 \[nucl-th\]](#).
- [71] Manjunath Omana Kuttan, Kai Zhou, Jan Steinheimer, Andreas Redelbach, and Horst Stoecker, “An equation-of-state-meter for CBM using PointNet,” *JHEP* **21**, 184 (2020), [arXiv:2107.05590 \[hep-ph\]](#).
- [72] Rui Wang, Yu-Gang Ma, R. Wada, Lie-Wen Chen, Wan-Bing He, Huan-Ling Liu, and Kai-Jia Sun, “Nuclear liquid-gas phase transition with machine learning,” *Phys. Rev. Res.* **2**, 043202 (2020), [arXiv:2010.15043 \[nucl-th\]](#).
- [73] Y. Nara, N. Otuka, A. Ohnishi, K. Niita, and S. Chiba, “Study of relativistic nuclear collisions at AGS energies from p + Be to Au + Au with hadronic cascade model,” *Phys. Rev. C* **61**, 024901 (2000), [arXiv:nucl-th/9904059](#).
- [74] Yasushi Nara, “JAM: an event generator for high energy nuclear collisions,” *EPJ Web Conf.* **208**, 11004 (2019).
- [75] H. Sorge, “Flavor production in Pb (160-A/GeV) on Pb collisions: Effect of color ropes and hadronic rescattering,” *Phys. Rev. C* **52**, 3291–3314 (1995), [arXiv:nucl-th/9509007](#).
- [76] H. Sorge, “Soft transverse expansion in pb(158 agev) on pb collisions: preequilibrium motion or first order phase transition?” *Physics Letters B* **402**, 251–256 (1997).
- [77] S.A. Bass, M. Belkacem, M. Bleicher, M. Brandstetter, L. Bravina, C. Ernst, L. Gerland, M. Hofmann, S. Hofmann, J. Konopka, G. Mao, L. Neise, S. Soff, C. Spieles, H. Weber, L.A. Winkelmann, H. Stöcker, W. Greiner, Ch. Hartnack, J. Aichelin, and N. Amelin, “Microscopic models for ultrarelativistic heavy ion collisions,” *Progress in Particle and Nuclear Physics* **41**, 255–369 (1998).
- [78] M Bleicher, E Zabrodin, C Spieles, S A Bass, C Ernst, S Soff, L Bravina, M Belkacem, H Weber, H Stöcker, and W Greiner, “Relativistic hadron-hadron collisions in the ultra-relativistic quantum molecular dynamics model,” *Journal of Physics G: Nuclear and Particle Physics* **25**, 1859–1896 (1999).
- [79] S. H. Kahana, D. E. Kahana, Y. Pang, and T. J. Schlagel, “Modeling relativistic heavy ion collisions at the AGS,” *Ann. Rev. Nucl. Part. Sci.* **46**, 31–70 (1996).
- [80] Bao-An Li and C.M. Ko, “Excitation functions of stopping power and flow in relativistic heavy-ion collisions,” *Nuclear Physics A* **630**, 556–562 (1998), nucleus-Nucleus Collisions.
- [81] Zi-Wei Lin, Che Ming Ko, Bao-An Li, Bin Zhang, and Subrata Pal, “A Multi-phase transport model for relativistic heavy ion collisions,” *Phys. Rev. C* **72**, 064901 (2005), [arXiv:nucl-th/0411110](#).
- [82] J. Weil et al., “Particle production and equilibrium properties within a new hadron transport approach for heavy-ion collisions,” *Phys. Rev. C* **94**, 054905 (2016), [arXiv:1606.06642 \[nucl-th\]](#).
- [83] N. G. Antoniou, F. K. Diakonos, A. S. Kapoyannis, and K. S. Kousouris, “Critical opalescence in baryonic QCD matter,” *Phys. Rev. Lett.* **97**, 032002 (2006), [arXiv:hep-](#)

- [ph/0602051](#).
- [84] A. Bialas and Robert B. Peschanski, “Moments of Rapidity Distributions as a Measure of Short Range Fluctuations in High-Energy Collisions,” *Nucl. Phys. B* **273**, 703–718 (1986).
- [85] E. A. De Wolf, I. M. Dremin, and W. Kittel, “Scaling laws for density correlations and fluctuations in multiparticle dynamics,” *Phys. Rept.* **270**, 1–141 (1996), [arXiv:hep-ph/9508325](#).
- [86] Nikolaos G. Antoniou and Fotios K. Diakonou, “Ising-QCD phenomenology close to the critical point,” *J. Phys. G* **46**, 035101 (2019), [arXiv:1802.05857 \[hep-ph\]](#).